HHS Public Access

Author manuscript

J Pharm Sci. Author manuscript; available in PMC 2021 January 01.

Published in final edited form as:

J Pharm Sci. 2021 January ; 110(1): 108–123. doi:10.1016/j.xphs.2020.09.008.

Preformulation Characterization and the Effect of Ionic Excipients on the Stability of a Novel DB Fusion Protein

Akshay Jain[a,b], **Gang Hu**[a,b], **Siva Sai Kumar Ratnakaram**[a], **David K. Johnson**[c], **William D. Picking**[a], **Wendy L. Picking**[a,**], **Charles Russell Middaugh**[a,b,*]

[a]Department of Pharmaceutical Chemistry, University of Kansas, Lawrence, KS 66047, USA

[b]Macromolecule and Vaccine Stabilization Center, University of Kansas, Lawrence, KS 66047, USA

[c]Computational Chemical Biology Laboratory, University of Kansas, Lawrence, KS 66047, USA

Abstract

Shigella ssp cause bacillary dysentery (shigellosis) which has high global morbidity in young children and the elderly. The virulence of *Shigella* relies upon a type III secretion system (T3SS) which injects host altering effector proteins into targeted intestinal cells. The *Shigella* T3SS contains two components, invasion plasmid antigen D (IpaD) and invasion plasmid antigen B (IpaB), that were previously identified as broadly protective antigens. When IpaD and IpaB were co-expressed to give the DB fusion (DBF) protein, vaccine efficacy was further improved. Biophysical characterization under various pH conditions showed that DBF is most stable at pH 7 and 8 and loses its conformational integrity at 48 and 50 °C respectively. Forced degradation studies revealed significant effects on the secondary structure, tertiary structure and conformational stability of DBF. In the presence of phosphate buffers as well as other anionic excipients, DBF demonstrated a concentration dependent conformational stabilization. Molecular docking revealed potential polyanion binding sites in DBF that may interact with phytic acid. These sites can be exploited to stabilize the DBF protein. This work highlights potential destabilizing and stabilizing factors, which not only improves our understanding of the DBF protein but helps in future development of a stable *Shigella* vaccine.

Keywords

Protein interactions; Protein formulation; Vaccine formulation; Anionic excipients; Cationic excipients; Biophysical stability; Biophysical characterization; Biologics stability; Forced degradation; Accelerated stability; Differential scanning calorimetry; Circular dichroism; Fluorescence spectroscopy; Shigella; Type III secretion system; Vaccine delivery

*Corresponding author. middaugh@ku.edu (C.R. Middaugh). **Corresponding author. wendy.picking@ku.edu (W.L. Picking).

Conflicts of Interest

None.

Appendix A. Supplementary Data

Supplementary data to this article can be found online at https://doi.org/10.1016/j.xphs.2020.09.008.

Introduction

Shigella spp. are Gram-negative bacterial pathogens responsible for approximately a half million cases of potentially severe dysentery (shigellosis) annually.[1] Across the genus, there are four species (*S. flexneri, S. sonnei, S. dysenteriae* and *S. boydii*) that include over 50 unique LPS-based serotypes with new serotypes still being identified. The type III secretion system (T3SS) is an essential virulence factor for all *Shigella* spp., as well as many other Gram-negative pathogens. *Shigella* uses its T3SS to promote bacterial entry in colonic epithelial cells as an early step in establishing infection.[2,3] Because the structural proteins of the T3SS are highly conserved among *Shigella* spp, those that are exposed are potential serotype-independent protective antigens. The *Shigella* T3SS contains two components, invasion plasmid antigen D (IpaD) and invasion plasmid antigen B (IpaB), that were previously identified as broadly protective antigens. Immunization with IpaD and IpaB alone or as a fusion protein (DBF) has demonstrated protective efficacy in a mouse model of infection.[4-7]

To develop a stable DBF protein based vaccine formulation, it is necessary to conduct a thorough biophysical characterization to evaluate the stability of the fusion protein under various physical and chemical stress conditions as a function of time.[8] For protein formulation development, forced degradation studies play a pivotal role by influencing candidate selection, storage conditions, assay development, and comparability studies. Here we investigated the individual effects of certain stress conditions such as pH, temperature, methionine (Met) oxidation, tryptophan (Trp) oxidation, and asparagine (Asn) deamidation on the biophysical characteristics of DBF. Evaluation of biophysical and biochemical properties of DBF under such conditions will also provide an improved mechanistic understanding of degradation effects on higher order structure, and a platform to characterize DBF for comparability assessment. In addition, the information from these assays will help to make rational decisions concerning formulation development, storage conditions and shelf life of the DBF protein for future development.

Apart from external stresses, protein-protein interactions, intramolecular interactions as well as protein ion interactions are known to have significant effects on a protein's conformational stability. Various salts (*e.g.* NaCl, Na_2PO_4),[9,10] cationic compounds and anionic compounds[11] have been widely explored for their effect on the conformational and colloidal stability of proteins. Anionic kosmotropes from the Hofmeister series often have a marked stabilization effect on folded proteins.[12] Ions may stabilize a protein by a variety of indirect hydration mechanisms.[13] Such mechanisms may be entropically driven to produce stabilizing effects. It has also been reported that some proteins follow a reverse Hofmeister series behavior due to their net charge,[14] which is in fact the result of their protein sequence and charged interacting sites. Researchers have also reported that proteins may electrostatically interact with ions at low concentrations resulting in destabilization, but then stabilize at higher ion concentrations. In one study, RNAse showed ion specific interactions at higher salt concentration that shielded electrostatic forces which stabilized the protein.[15] We therefore explored various charged excipients to evaluate their interaction and stabilization effects on DBF. Many degradation pathways such as deamidation or oxidation are dependent on the conformational flexibility, solvent exposure, pH, and temperature.

Optimizing the solution conditions with stabilizing salts or excipients can inhibit such degradation pathways. In this study, we evaluated phosphate buffer and several anionic and cationic excipients for their binding and stabilization effects on the DBF protein. In addition to the charged excipients, conventional GRAS (generally recognized as safe) excipients such as sugars, polyols, and surfactants were also examined. This work can serve as an initial foundation for future development of a stable and highly efficacious DBF protein formulations.

Material and Methods

Protein Preparation

Construction of the plasmid containing the gene for the DB Fusion (DBF) and the protein purification methods have been reported earlier,[5] except for the modifications described here. DBF expression strains were grown in a fed-batch mode using a 10 L bench top bioreactor (Labfors 5, Infors USA Inc. MD) equipped with polarographic dissolved oxygen sensor (pO2), pH probe (Hamilton Company) and advanced fermentation software. Media, trace elements and other chemicals were prepared as per the manual provided by Infors USA Inc. [Annapolis Junction, MD]. Briefly, preculture fluid was prepared by inoculating ~25 μL aliquots of frozen glycerol stock into 50 mL of 1× Lysogeny broth (LB) supplemented with chloramphenicol (34 μg/mL) and allowed to grow overnight at 30 °C with shaking at 200 rpm. The inoculum was made by transferring cells from a pre-culture to a 1000 mL of Terrific broth (TB) medium with the same antibiotic and grown at 30 °C until reaching an OD 600 nm of ~2.5. In the next step, ~700 mL of inoculum was transferred to the sterilized fermenter containing 8 L of the TB medium with appropriate antibiotics. The culture temperature was maintained at 30 °C and pH 7. Other parameters like stirrer speed, gas mix, and flow were set in cascade mode as a function of pO2 (40%). DBF/*ipgC* expression was induced by addition of 1 mM IPTG at an OD600 nm of ~25. After 3 h, bacteria were collected by centrifugation, washed and resuspended in IMAC binding buffer (20 mM Tris pH 7.9, 500 mM NaCl, 10 mM imidazole) having 0.1 mM 4-(2-aminoethyl) benzenesulfonyl fluoride hydrochloride (AEBSF) and lysed in a microfluidizer at 18,000 psi with three passes. The cellular debris was removed by centrifugation at 10,000 g for 30 min and the supernatant containing the protein complex was purified as per the procedure reported earlier.[3] The molecular weight of DBF is 99,057 Da with extinction coefficient of 48,360 M^{-1} cm^{-1}, at 280 nm. LPS levels were determined using a NexGen PTS with EndoSafe cartridges (Charles River Laboratories) and was <5 EU.

Far-UV Circular Dichroism (CD)

CD Spectra in the far UV region were obtained using a Chirascan-plus CD Spectrophotometer (Applied Photophysics, UK) equipped with a Peltier controlled six cell holder. DBF (0.1 mg/mL) was loaded into a 1-mm quartz cuvette and spectra were obtained in the far UV region (190—260 nm) in 1 nm increments with 1 s per data point integration time. To evaluate thermal melting, a temperature ramp was imposed from 10 to 90 ° C (acquisition at every 2.5 °C) with an equilibration of 2 min at each temperature. After acquisition at 90 °C, DBF protein samples were cooled to 10 °C and rescanned.

Intrinsic Tryptophan Fluorescence

A fluorescence plate-reader (Fluorescence Innovations, Minneapolis, MN) equipped with a tunable pulsed dye laser, a temperature controlled 384-well sample holder (Torrey Pines Scientific, Carlsbad, CA), and a high-speed digitizer was used to obtain Intrinsic tryptophan fluorescence spectra. Experimental samples were loaded into a Hard-Shell 384-well PCR plates. Two microliter silicon oil (Thermo Fisher Scientific, Waltham, MA) was added to prevent sample evaporation during temperature ramps. Samples were excited at 295 nm and steady state emission spectra were collected using a charged coupled device detector from 310 nm to 400 nm. Fluorescence moment (mean center of spectra mass peak position or MSM peak position) was reported. Temperature ramps were set from 10 to 95 °C with an increment of 1 ° C per step and an equilibration time of 60 s at each temperature. Moment (MSM peak position) were plotted as a function of temperature and first derivative of the resulting data was used to calculate the melting temperature (T_m) using Origin 7.0 (OriginLab; Northampton, MA).

Differential Scanning Calorimetry (DSC)

DBF protein samples (0.4 mg/mL) under various experimental conditions were evaluated for thermal and overall conformational stability with a MicroCal VP-Capillary DSC (Malvern, UK). DBF protein samples (400 μL) were added into a 96 well plate and stored in a temperature controlled (5 °C) auto-sampler. Samples were scanned from 10 to 110 ° C at a 1 °C/min rate. The acquired data was analyzed and processed using Origin 7.0 software (OriginLab; Northampton, MA).

Fourier-Transform Infrared (FT-IR) Spectroscopy

A Tensor-27 FT-IR spectrometer (Bruker, Billerica, MA) equipped with a Bio-ATR cell was used for FT-IR spectroscopic analysis. Liquid nitrogen was used to cool the detector and a continuous N_2 gas flow was used to purge the interferometer. A total of 256 scans were recorded from 4000 to 900 cm^{-1} at a 4 cm^{-1} resolution at 10 °C. The background spectra from each experimental buffer condition were subtracted from the sample spectra. Acquired spectra were processed for atmospheric compensation, baseline adjustment, and normalization by OPUS V6.5 (Bruker, Billerica, MA) software. Deconvolution of the amide I region of the acquired spectra from various experimental conditions were performed by Python script where the data set was processed by mixed Gaussian/Lorentzian bands. Similarly, the second derivative of each spectrum was calculated, and peaks were identified for secondary structure content.

DBF Protein Sample Preparation

To evaluate the effect of pH, DBF protein (1 mg/mL) was buffer exchanged into citrate-phosphate buffer ranging from pH 4 to 8 by Amicon® Ultra Centrifugal Filters of 30 KDa molecular cut-off (MilliporeSigma™). All samples contained 0.05% Lauryldimethyl-amine *N*-oxide (LDAO) as described previously.[3] After 2 h of incubation at room temperature, samples were analyzed for conformational and thermal stability using CD and DSC.

DBF protein in 20 mM MOPS buffer (0.05% LDAO) was prepared and divided into three groups. One group was kept as control with no phosphate and the other two groups were

supplemented with sodium phosphate to achieve 1, 10, and 100 mM final phosphate concentration. Similarly, DBF was also formulated with increasing NaCl (1,10 and 100 mM) concentration to examine the impact of ionic strength on the stability of DBF.

Forced Degradation of DBF Protein

To evaluate methionine oxidation, H_2O_2 (3% w/w) was added to the DBF stock solution. The resulting solution was aliquoted into 4 groups (n = 3). Each group was evaluated for the effect of temperature (4 °C and 37 °C) and time (at days 2 and 5) on the oxidation of DBF. After each individual timepoint (days 2 and 5), 200 mM Met solution was added to quench the oxidation reaction. DBF protein formulated in 20 mM MPOS, 0.05% LDAO, pH 7.4 was used as control and incubated at 37 ° C for five days. Protein samples were then buffer exchanged into 20 mM MOPS (0.05% LDAO) at 7.4 pH, aliquoted, and frozen at −80 °C until evaluation.

Tryptophan oxidation was performed by incubating the DBF protein with 2,2′Azobis (2-methylpropionamidine) dihydrochloride (AAPH; 2 mg/mL). The molar ratio of protein:AAPH was kept at 1:100. To protect the Met residues in DBF from oxidation, DL-Met (10 mg/mL) was added to the solution. The resulting solutions were divided into the groups described above. After each timepoint, the samples were buffer exchanged into 20 mM MOPS (0.05% LDAO) at 7.4 pH, aliquoted, and stored at −80 °C until evaluation.

To achieve Asparagine (Asn) deamidation, stock DBF protein was buffer exchanged into Tris buffer (pH 9.5). After mixing, the solution was aliquoted and stored at 4 °C or 40 °C. At various timepoints such as Day 3, 5, and 7, samples were collected and buffer exchanged in 20 mM MOPS (0.05% LDAO) at 7.4 pH, aliquoted, and stored at −80 °C until evaluation. DBF protein formulated in 10 mM MPOS, 0.05% LDAO, pH 7.4 was used as control and incubated at 40 °C for seven days.

SDS-PAGE

Samples from forced degradation studies such as Asn deamidation, Met oxidation, and Trp oxidation were mixed with 4× laemmli buffer with or without dithiothreitol (DTT). Control, reduced, and non-reduced protein samples were heated at 90 C for 10 min. After centrifugation at 14,000×*g* for 2 min, 20 μL of samples were loaded into the wells of NuPAGE™ 4—12% Bis-Tris Protein Gels. Samples were run for 75 min at 150 V in NuPAGE MOPS SDS Running Buffer. Gels were stained with Coomassie blue and destained with water before imaging.

Hydrophobic Interaction Chromatography

Separation of DBF protein based on the hydrophobicity was performed using a TSKgel Phenyl-5PW, 10 μm, 7.5 mm ID × 7.5 cm column and Shimadzu HPLC system. DBF protein samples from various groups were diluted to 2 mg/mL in 50 mM Phosphate buffer (pH 7.4), 0.05% LDAO, pH 7.4 and mixed with equal volumes of 2 M ammonium sulfate solution. The resulting 1 mg/mL DBF was injected into the column equilibrated with Phosphate buffer (elution buffer). After an initial 4 min isocratic step of 1 M ammonium sulfate run, followed by a negative gradient of 1 M ammonium sulfate was run for 20 min at

a flow rate of 0.5 mL/min, to elute the DBF protein based on their retention behavior (hydrophobicity). Area under the curve was calculated for each peak between the void volume and end of run. The chemically modified species were reported in percent.

Imaged Capillary Isoelectric Focusing

To evaluate the charge variants of DBF protein after forced deamidation at pH 9.5, capillary isoelectric focusing was performed. DBF protein samples were diluted in water to 1 mg/mL. The protein was mixed with 1% methyl cellulose (ProteinSimple), 3—10% Pharmalyte (GE Healthcare), 500 mM DTT (DL-Dithiothreitol) (Sigma Aldrich), and appropriate pI markers of 4.6 and 9.5 (ProteinSimple). Next, the diluted samples were injected into a fluorocarbon-coated capillary cartridge using an iCE3 (ProteinSimple) system autoinjector. Samples were prefocused for 1 min at 1500 V and then focused for 5 min at 3000 V followed by wash period of 90 s. The focusing patterns were then captured by a CCD camera at 280 nm.

Size Exclusion Chromatography

Size exclusion chromatography was used to investigate the formation of higher molecular weight species (aggregates) and low molecular weight species (fragments) after forced degradation of DBF protein. A Shimadzu HPLC system was used equipped with UV—vis (214 nm and 280 nm) and fluorescence detector (excitation = 295 nm and emission = 330 mn). Samples were diluted in 50 mM Phosphate buffer (pH 7) and injected with the help of autoinjector in a TSKgel G3000SWXL column (7.8 mm × 300 mm) along with a TSKgel SWXL guard column (6.0 mm × 40 mm) from Tosoh Bioscience (King of Prussia, PA). The flow rate was kept 0.7 mL/min, and samples were held at 5 ° C in the auto sampler.

DBF Protein Binding to Alhydrogel

DBF proteins solutions were prepared in various concentrations ranging from 2.5 mg/mL to 0.075 mg/mL. DBF protein solution was added to Alhydrogel stock of 2 mg/mL, prepared in MOPS buffer (0.05% LDAO) supplemented with various phosphate concentrations at a 1:1 (v/v) ratio to achieve a final Alhydrogel concentration of 1 mg/mL. The samples were mixed by vortexing and incubated at room temperature for 24 h. Suspension was resuspended by vortexing and centrifuged at 2000×*g* to separate the unbound DBF protein from Alhydrogel. Unbound DBF protein was quantitated from the supernatant using bicinchoninic acid (BCA) assay.

After determining the concentration of free DBF protein (C_e), the amount of bound DBF protein (C_o) was calculated (C_o—C_e). The amount of bound DBF protein per mg of aluminum (Q_e) was calculated by dividing C_o—C_e by the amount of Alhydrogel used (i.e., 50 mg). Finally, Langmuir isotherms were generated by plotting Q_e vs C_e and the linear form of the isotherm obtained by plotting C_e/Q_e vs Ce. The linear form of the Langmuir isotherm was further analyzed to obtain the adsorptive capacity (Q_m) from the slope and adsorptive/Langmuir coefficient (KL) from the y intercept of the fitted straight line.

Size and Zeta Potential

DBF protein formulated with varying concentrations of phosphate buffers was evaluated for its effect on the size and zeta potential of the Alhydrogel based formulation. Alhydrogel and

DBF protein were formulated in 20 mM MOPS buffer (0.05% LDAO) supplemented with various phosphate concentration (1, 10 and 100 mM). The resulting suspension was analyzed in a Malvern Helix instrument (Malvern Instruments, Malvern, UK) for average zeta potential. One mL of sample was placed in a plastic disposable capillary cell with gold electrodes and zeta potentials measured with a 632 nm laser in a 173° backscatter configuration. The measurements were performed for three independent samples with six analytical replicates each.

The size distribution of the DBF-Alhydrogel suspension formed in the presence of different phosphate concentrations was determined by using a Malvern Mastersizer 3000 (Malvern Instruments, Malvern, UK). Background measurement was taken by adding 6 mL of dH2O to the sample chamber. Three hundred microliter of Alhydrogel-DBF (Alhydrogel at 1 mg/mL) formulation sample was injected for each measurement to achieve ~4% total light obscuration. A refractive index of 1.57 was used for Alhydrogel in Mie scattering calculations for the determination of size. Size distributions were reported by number percent. Three individual replicates were measured for each sample with an average of ten analytical replicates for each run.

Effect of Anions and Cations on Stability of DBF Protein

DBF protein stock solution (1 mg/mL) was mixed with anionic or cationic excipients at 10× and 0.5× (by weight) concentrations with respect to the protein concentration. Final concentration of protein was maintained at 0.5 mg/mL. Anionic excipients used in the study were dextran sulfate, heparin sulfate and phytic acid whereas, cationic excipients used in this study were polyarginine, Protamine, and 1,4-Diaminobutane dihydrochloride (DABC or Putrescine dihydrochloride). The solution mixtures were incubated at room temperature for 2 h before investigation.

Molecular Docking of DBF Protein

Structures of IpaD, PDB ID's 3R9V[16] and 5VXJ,[17] and IpaB, PDB ID 5WKQ,[18] were downloaded and prepared using the Schrodinger Protein Preparation Wizard to add hydrogens, identify protein protonation states, optimize hydrogen bonding, and so forth.[19] The protonation state of phytic acid were predicted using LigPrep as well,[19] with one of the three states being dramatically better than the others. The hydrogen bond optimized structures, along with phytic acid, were prepared using AutoDockTools, and grid dimensions that would contain the entire protein were identified. Phytic acid was docked into each structure 1000 times with an exhaustiveness setting of 10. Of the 10,000 poses reported, the top 1000 were retrieved to identify potential sites for further exploration. Additionally, with IpaB, other potential sites were identified by visual inspection for clusters of cationic residues.

Docking was performed at each site using Schrodinger Glide with extended precision (XP), with the top 10 poses for each ligand state maintained.[20-22] To enhance the sampling, the following settings were changed from default: 50,000 poses per ligand in the initial docking phase, a scoring window of one thousand, one thousand poses were kept for minimization of initial poses, enhanced sampling was selected, and 20 post-docking minimizations were

performed. Additionally, intramolecular hydrogen bonds were rewarded. For the sites that had poses, the top scoring unique poses were refined using Prime.[23,24]

Excipient Screening

Select FDA approved pharmaceutical excipients for parenteral injection (listed in the FDA inactive ingredient guide 28) were screened. These excipients included salts, polyols, alcohols, sugars, detergents, proteins, amino acids, and polymers. DBF protein (1 mg/mL) was mixed with respective excipients and incubated at 4 °C overnight. List of excipients and concentrations are listed in the supplementary Table 2.

Statistical Analysis and Graphing

GraphPad Prism 8 software (San Diego, CA) was used for statistical analysis. All data were presented as mean ± SD. Comparison between three or more groups was performed using a one-way analysis of variance (ANOVA) with Tuckey's Post Hoc test. $p < 0.05$ was considered statistically significant.

Results and Discussion

Effect of pH on Secondary Structure of DBF

The Far-UV CD spectra of DBF shows double minima at 208 nm and 222 nm (Fig. 1A), suggesting dominance of alpha helical secondary structure when formulated with 20 mM MOPS and 0.05% LDAO. The CD spectra showed a similar double minima shape at pH 6, 7, and 8. At pH 4 and 5, however, diminishing (almost total loss) of minima at 208 nm suggested extensive conformational changes of DBF at acidic pH values. Such loss of a 208-nm minimum is assumed to reflect extensive loss of α helical structure.[25] This is confirmed by the loss of negative ellipticity at 222 nm minimum, further reflecting major conformational changes at acidic pH. The CD spectra from each sample at various pH conditions were deconvoluted and secondary structure content were quantitated using the BeStSel program.[26] As shown in Fig. 1B, regular α helical (helix 1) structures were absent in DBF at pH 4 and 5. Moreover, the regular a helical (helix 1) content increased significantly from pH 5 to 8. At pH 4—60, nearly 5—6% distorted helical structures were observed in comparison to >15% at pH 7 and 8. In addition, a significant rise in β turn content suggests extensive conformational changes in DBF at acidic pH. Some visible precipitation was also observed at pH 4, 5 and 6 (data not shown).

The CD signal at 222 nm was monitored for each individual pH group (pH 4 to 8) at temperatures from 10 to 90 °C to evaluate the effect of temperature on the overall secondary structure stability of DBF (Fig. 1C). A decrease in negative ellipticity was observed in all the samples as a function of temperature with different unfolding patterns. DBF protein demonstrated single thermal transition at ~42 ° C with a melting temperature (T_m) of ~48 and 50 °C at pH 7 and 8 respectively, whereas at pH 4 no thermal transition was observed. Despite significantly lower molar ellipticity, DBF showed a small transition at 52 °C at pH 5. These observations indicated the need for neutral to slightly basic pH for conformational stability of DBF.

Effect of pH on Thermal Stability of DBF Protein

To investigate the thermal and conformational stability of DBF at various pH conditions, differential scanning calorimetry (DSC) was performed. Fig. 1D illustrates the baseline corrected thermograms of DBF protein at pH 6, 7, and 8. The T_m of DBF at pH 7 and 8 was observed to be 47.9 and 50.2 ° C respectively. In contrast, a minor thermal transition was observed with a T_m close to 80 ° C at pH 6. No thermal transitions were observed at the lower pH values.

Forced Oxidation of DBF Protein

Major oxidation sensitive amino acids include His, Met, Cys, Tyr, and Trp. In the present study, protein was incubated with hydrogen peroxide (H_2O_2) and 2,2′-Azobis (2-methylpropionamidine) dihydrochloride (AAPH) that can selectively modify Met and Trp residues respectively. AAPH also generates alkyl radicals that catalyze the formation of reactive oxygen species, which often oxidizes Trp residues. Such oxidations can arise from many sources during formulation development, storage, or transportation. The resulting degradants can alter bioactivity and the conformation of therapeutic proteins.[8,27] Control DBF was examined by non-reducible SDS-PAGE and multiple high molecular weight species (HMWS) were observed after exposure to AAPH or peroxide (Fig. 2A). These self-associated HMWS were found to be reducible by DTT (Fig. 2B), resulting in singular band for the DBF protein. This suggests that intermolecular covalent disulfide interactions are responsible for formation of the HMWS for DBF. For future formulation development, successful masking of these cysteine molecules by adding reducing agent may inhibit these covalent interactions.

It is known that depending on the incubation temperature, H_2O_2 may form hydroxyl radicals or superoxide anion radicals.[28] Therefore, we conducted degradation studies at two different temperatures, 4 °C and 37 °C. In presence of H_2O_2 and AAPH, the bands on SDS PAGE protein gels appeared consistent with the control at 4 °C incubation (Fig. 2). In contrast, incubation at 37 °C showed significant degradation. This suggests that the rate of Met and Trp oxidation mediated degradation are highly temperature dependent. Protein bands produced by Met oxidation show a linear trend of diminishing protein gel band intensity with time. As shown in Fig. 2, degradation of BDF protein due to H_2O_2 mediated Met oxidation at 37 °C increased significantly from day 2—5. In addition, AAPH mediated Trp oxidation resulted in formation of higher molecular weight species (probably aggregates) that did not migrate into the gel and remained at the gel interface (Fig. 2). This data shows that the surface exposed Trp residues that are easily accessible to the external environment containing AAPH are significantly altered, which led to aggregation of the DBF protein. Fluorescence emission spectra of DBF showed an early MSM fluorescence peak at 345 nm at 10 °C suggesting partially surface exposed Trp residues (Fig. 4, Spectra not shown) at both incubation samples (4 °C and 37 °C). Apparently, 37 °C incubation resulted in higher AAPH exposure and a higher degree of degradation on day 2 at 37 °C. This is evident in the fluorescence melt curve (Fig. 4) and SDS PAGE analysis (Fig. 2A and B).

Next, we used hydrophobic interaction chromatography to evaluate the extent of oxidized DBF protein in presence of H_2O_2 and AAPH. As shown in Fig. 2C and D, DBF protein

incubated with H_2O_2 at 4 °C showed no significant difference in oxidation species formation on Day 5 in comparison to the control sample. Although, AAPH showed greater degradation at 4 °C compared to samples incubated with H_2O_2, the difference on Day 5 was not significant. In contrast, DBF incubated with H_2O_2 at 37 °C and AAPH at 37 °C resulted in nearly 6—8% oxidation on day 5. This also agrees with the SDS-PAGE analysis and demonstrates that the extent of oxidation is highly temperature dependent.

Size exclusion chromatography (SEC) was used to further evaluate the impact of oxidation and higher temperature on the aggregation of the DBF protein. In comparison to the control, DBF incubated with AAPH demonstrated significantly higher aggregation. As shown in Fig. 2F, High molecular weight species (HMW) increased to ~60% in presence of AAPH on day 5. In contrast, H_2O_2 incubated samples resulted in approximately 18% HMW species formation on day 5. This data confirmed the statement above that Trp oxidation leads to greater degree of aggregation in DBF in comparison to the Met oxidation.

We compared the far-UV CD spectra of Met oxidized (H_2O_2) DBF protein with the unmodified DBF (To) and control DBF incubated at 37 °C for 5 days to examine for potential conformational changes. The slight increase in negative ellipticity with H_2O_2 oxidation suggests small secondary structural changes (Fig. 3A). Deconvolution of the CD spectra revealed a small increase in a helical content from ~15% to ~20% at both temperatures (Fig. 3B). In the presence of AAPH, the negative ellipticity changed at every incubation temperature and time point. This also suggests conformational changes with time (Fig. 3C). Deconvolution of the spectra revealed that the α helical content increased after 2 days of incubation in AAPH but leveled back to the control values on day 5 at both temperatures (4 °C and 37 °C). In the presence of AAPH, antiparallel β structures increased under both temperature conditions and time points suggesting that the oxidation of Trp residue has greater conformational impact on the DBF protein than Met oxidation.

Effect of Oxidation on the Tertiary Structure of DBF

To evaluate the effect of oxidation on the tertiary structure stability of DBF, the intrinsic tryptophan fluorescence moment as a function of temperature was monitored. The goal of this study was to examine the changes in the unfolding pattern of DBF after selective forced oxidation. DBF contains four Trp residues located in the IpaD portion (W135, W177, W226, and W279) and one Trp residue in the IpaB portion (W439). As shown in Fig. 4A-D, DBF at T0 showed no intrinsic Trp fluorescence melting transition after various forms of oxidation as a function of temperature. This is consistent with previously published report.[3] In contrast, DBF incubated with H_2O_2 and AAPH showed a consistent early thermal transition at 33.9 °C at both incubation temperatures (4 °C and 37 °C) and timepoints (Day 2 and 5) suggesting a destabilization effect of oxidation. A second thermal transition observed at 73—74 °C was also present at all incubation temperatures and time points except for DBF treated with AAPH at 37 °C for 5 days. Moreover, for AAPH oxidized samples, the thermal transition patterns were different on day 5 of incubation at 4 °C and 37 °C. In the 4 °C group, after the first thermal transition at ~33 °C, a significant blue shift was observed which plateaued at ~341 nm followed by a second transition at 80.9 °C (Fig. 4C). This significant blue shift and increase in the second transition may be attributed to the change in the Trp

microenvironment to a relatively more hydrophobic region in the three-dimensional structure of DBF. The blue shift was even more significant in samples at day 5, which was restored after the second thermal transition at ~60 °C(Fig. 4D). A red shift followed by a blue shift could possibly be the result of change of microenvironment of Trp at different temperatures and a 2-phase unfolding of protein. At the first thermal transition, Trp moved to the relatively non-polar interior of the protein resulting in a blue shift followed by another transition at 60 °C resulting in restoration of Trp to more polar exterior microenvironment. This study suggests that the Trp residues in particular regions play a vital role in the conformational stability of the DBF protein and should be protected by formulation strategies.

Forced Deamidation of the DBF Protein

Deamidation of Asn residues under basic pH conditions form succinimide, which upon hydrolysis yields aspartate (Asp) and isoaspartate residues (IsoAsp). In addition to forming acidic isoforms, this reaction may lead to covalent crosslinking. To study the effect of deamidation on formation of reducible and non-reducible cross-linked species, SDS PAGE was used (Fig. 5A). As discussed previously, DBF forms covalent cross-linked disulfide species having a higher molecular weight. These crosslinked species were easily reduced with DTT as shown in Fig. 5B. Despite reduction with DTT, sharp bands of dimer species were visible at 4 °C incubation samples. This suggests the presence of noncovalent interactions. As shown in Fig. 5A and B, cumulative DBF protein band intensity kept decreasing with time at both incubation conditions (4 °C and 40 °C). Moreover, lower molecular weight bands begin to appear on day 3 (40 °C) with diminishing main band intensity as a function of incubation time (Fig. 5A and B). This suggests that the deamidation of DBF is temperature dependent with a lower rate of degradation at 4 °C incubation.

Aggregation propensity of DBF due to deamidation stress was evaluated by SEC. In comparison to the control samples, DBF incubated at pH 9.5 demonstrated similar trend of aggregation. In fact, it was evident that the aggregation of DBF is temperature dependent, not pH (Fig. 5C and D). Both samples, incubated in pH 7.4 and 9.5, demonstrated approximately 58—60% HMW species on day 7. At 4 C, DBF incubated at 9.5 pH showed 8% HMW species (Data not shown).

To evaluate the presence of acidic species (Asp or IsoAsp) after deamidation of DBF at pH 9.5, capillary isoelectric focusing (cIEF) was used. After 3 days of incubation in pH 9.5 at 40 °C, ~25% of DBF resulted in acidic species (Fig. 5 E). This deamidation trend increased with time and reached 43% on day 7. The rate of deamidation was significantly lower in case of lower temperature (4 °C). Only 8.3% acidic species were formed after 7-day incubation at 4 °C in pH 9.5. Interestingly, control DBF incubated in pH 7.4 at 40 °C showed no deamidation until day 7. Acidic species percent grew from zero to 24% on day 7 (Fig. 5 E). This data also suggests that the temperature plays an important role in the degradation of the DBF protein.

Effect of Deamidation on Higher Order Structure

Secondary structure may also be affected by the modification of Asn residues and their deamidation, which may impact the stability of the protein. Using circular dichroism, we investigated the changes in the secondary structure of DBF protein after forced deamidation conditions (Fig. 6). At both temperatures (4 °C and 40 °C), a reduction in negative ellipticity was observed, which suggests enhanced disorder in the secondary structure of DBF (Fig. 6A and C). At 4 °C and 40 °C, the regular helical and distorted helical content decreased with time until. The opposite trend was observed with respect to the β structures. Parallel and anti-parallel β structures increased with time. In comparison to the T_0 sample, the minimum at 208 nm showed a more pronounced reduction with time. Deconvolution of the CD spectra revealed that a reduction in α helical content and an increase in right twisted anti-parallel β structures, indicating a major conformational change during deamidation at 40 °C with incubation time. DBF control incubated at 40 °C in pH 7.4 showed no significant changes in comparison to the T_0 sample.

The intrinsic tryptophan fluorescence moment as a function of temperature was plotted for DBF at various incubation times (Fig. 7). All samples showed a consistent thermal transition at 34 °C observed in oxidized samples, whereas control DBF showed no thermal transitions. At 4 °C (Fig. 7A), the fluorescence moment undergoes a blue shift as temperature rises from 34 °C. This plateaued at 60 °C and 324 nm suggesting Trp sidechain movement to a more hydrophobic region. On day 5, although having a similar thermal transition, the blue shift plateaued at 65 °C and 335 nm. This relative red shift indicates that the protein undergoes significant tertiary structural rearrangements with time leading to different thermal unfolding pattern. Interestingly, on day 7, the thermal unfolding event restores as day 3. Under 40 °C conditions (Fig. 7B), two distinct and consistent thermal transitions were observed at ~33 °C and 75 °C. The thermal unfolding pattern of Day 3 and day 5 are almost identical, where the blue shift after the first transition plateaus at 50 °C and 346 nm. Interestingly, on day 7, the blue shift after the first thermal transition plateaus at 49 °C and 344 nm. This relatively higher blue shift of samples incubated for 7 days suggest greater tertiary structural alterations in comparison to day 3 and 5.

Effect of Phosphate on DBF Protein Stability

The DBF protein was formulated in 20 mM MOPS (0.05% LDAO) with varying amounts of phosphate to evaluate the effect of anionic phosphate on the stability of DBF. Thermal stability of the resulting formulations was examined using differential scanning calorimetry. As shown in Fig. 8A and B, the melting temperature (T_m) increased from ~50 °C to 57.5 °C with linearly increasing phosphate concentration (1,10 and 100 mM) in the solution. Such a significant increase in T_m can be attributed to an ionic strength effect, Debye Hückle charge shielding or binding of phosphate ions to the DBF protein.

The effect of phosphate on the secondary structure of the protein was also evaluated by circular dichroism (CD). Fig. 8C shows the mean residue ellipticity (MRE) of DBF formulated in different phosphate concentrations. DBF showed a distinctive double minimum in the presence of phosphate with only slight changes in molar ellipticity. The negative molar ellipticity of DBF increased with increasing phosphate concentrations. This

is indicative of formation of more ordered secondary structure. The minimum at 222 nm did not change with further increases in phosphate concentration, but significant change was observed at the 208 minimum. A pronounced 208 nm band suggests significant conformational changes in the α domain of DBF after interaction with phosphate anion. To examine the effect of phosphate on thermal stability, the ellipticity at 222 nm as a function of temperature was monitored in presence of different phosphate concentrations (Fig. 8D). The Tm increased by approximately 4 °C, suggesting a thermal stabilization effect by 10 mM phosphate. In contrast, the T_m value increased by only 1° when the phosphate concentration increased from 10 to 100 mM. This suggests the saturation of binding sites by phosphate ions. The change in ellipticity was also monitored at 208 nm as function of temperature. As shown in Fig. 8E, DBF in absence of phosphate showed multiple small transitions which reduced with increasing phosphate concentration in solution. This demonstrates that the phosphate anions provide conformational stability to the DBF protein by affecting the early thermal transitions of the protein.

To see if this stabilization is an ionic strength or Debye Huckle charge shielding effect, we incubated the DBF protein with increasing concentrations of NaCl (10 and 100 mM). As shown in Fig. 8F and G, the Tm values reduced slightly with increasing NaCl concentration, suggesting strongly that the stabilization was, in fact, the result of phosphate ion interacting with anion binding sites within DBF. After the thermal melting analysis up to 90 °C at various phosphate concentrations, DBF (with 0.05% LDAO) samples were cooled back to 10 °C and CD spectra was acquired (Fig. S1). Both spectra, before and after thermal unfolding, were superimposable suggesting that the DBF protein retains its secondary structure as described previously by Chen et al.[3] It is also noteworthy that inclusion of phosphate does not influence this refolding behavior.

As phosphate binding provided thermal and secondary structure stability, FTIR was used to quantitate the secondary structure content. The FTIR spectra of the amide I region was deconvoluted for quantitation. As shown in Fig. 9 A-B, the secondary structure did not change with 10 mM phosphate addition to the solution. In contrast, significant changes in the secondary structure were observed at 100 mM phosphate concentration. The α helical content significantly reduced from ~45% to ~37% and β sheet content doubled from ~14% to 28% in 100 mM phosphate. Deconvoluted FTIR spectra in Fig. 9 (100 mM Phosphate) showed increased intramolecular β structures (1631—1626 cm^{-1}). We believe that this trend would have increased with further increase in phosphate concentration in the formulation. This can be attributed to stronger intramolecular hydrogen bonding. Although, we did not investigate further increase in the phosphate ion, we presume that the protein would start to aggregate or precipitate. Researchers have demonstrated that the shifting of β structures to lower wavenumber is attributed to the inter or intramolecular β-sheet structures leading to aggregation of the molecule.[29] Interestingly, phosphate binding also resulted in slight decrease in the hydrodynamic radius of the DBF protein, but the change of statistically insignificant (Fig. 9C).

Another possible explanation could be that the salts affect proteins' structural stability by either interacting with the protein or by changing the water structure. We demonstrated that phosphate interacts with the DBF protein but due to kosmotropic nature of the phosphate

ions (Hofmeister series), at higher concentration water hydration structure formation is inhibited. This results in dehydration and increased intermolecular interactions. However, we did not notice any enthalpic change (ΔH) due to phosphate concentration.

Effect of Phosphate on DBF Protein Binding on Alhydrogel

In the presence of anions, such as phosphate, modulation of the surface charge of the adjuvant Alhydrogel can be achieved.[30] We therefore anticipated that the presence of anions such as phosphate in the DBF protein formulation would have an impact on its binding to Alhydrogel. We added DBF protein (0.05% LDAO) with 0, 10, and 100 mM phosphate to Alhydrogel. As expected, a decrease in the binding of DBF protein to Alhydrogel was observed with increasing phosphate concentration (Fig. S2A-B). The nonlinear curve generated by increasing the DBF amount added versus DBF amount bound was fitted and the binding affinity and binding capacity were calculated using a Langmuir isotherm (Fig. S2B). A decreasing trend of DBF protein binding affinity and binding capacity toward Alhydrogel was also observed with increasing phosphate concentration (Fig. S2 C-D). Although, 0 mM and 10 mM phosphate groups were statistically insignificant in terms of binding affinity and capacity.

The surface properties of the Alhydrogel in the presence of phosphate were also analyzed. The mean particle diameter was approximately 1.5 μm at all phosphate concentrations except 1 mM phosphate the where size increased to ~2.4 μm (Fig. S3 A-B). The change in size is attributed to the surface zeta potential of the Alhydrogel in the presence of different phosphate concentrations. In the absence of phosphate, the zeta potential was observed to be ~16.2 mV, which reached approximately −30 and −25 mV at 10- and 100-mM phosphate concentrations, respectively (Fig. S3 C). At 1 mM phosphate, however, the Zeta potential was near neutral, i.e. +0.4 mV. At neutral charge, the attractive force among particles dominates and results in larger particles at 1 mM phosphate concentration. In contrast, at 0, 10- and 100-mM phosphate concentration, repulsive forces dominated and led to smaller sizes.

Effect of Polyanions on the Stability of DBF Protein

To validate the stabilization of DBF protein structure by various anionic phosphate molecules, we investigated few anionic excipients such as sulfated polysaccharides (heparin sulfate and dextran sulfate) and a phosphate rich small molecule (phytic acid). We hypothesized that the DBF protein has certain anion binding sites that upon binding with anions favors structural stability. Anionic excipients at varying concentrations, 0.5× and 10× (by weight), were incubated with DBF. DSC analysis (Fig. 10) revealed that each molecule had a unique thermal stabilizing effect. Dextran sulfate and Heparin sulfate, being larger polyanionic molecules produced a significant increase in T_m at 0.5× concentration. Phytic acid, however, showed a concentration dependent stabilization effect, increasing the T_m by 1.8 °C and 7.8 °C at 0.5× and 10× concentrations, respectively. The data shown in Fig. 10A and B suggests that the larger polyanionic molecules such as dextran sulfate and heparin were highly effective at lower concentrations (0.5×) in improving the physical stability of the protein. To explore this phenomenon, concentration dependent thermal unfolding was monitored in the presence of phytic acid. As shown in Fig. 10 F, the T_m as a function of

phytic acid (ligand) concentration showed a non-linear thermal stabilization pattern with escalating ligand concentration. The T_m values gradually increased from 50 °C at 0.25 mg/mL to 57.5 °C at 20 mg/mL phytic acid concentration. In contrast, dextran sulfate demonstrated very efficient thermal stabilization as the T_m reached 56 °C at 0.02 mg/mL concentration and plateaued at 57 °C at 0.3 mg/mL concentration (Fig. S4). This shows a remarkable stabilization effect of larger anionic excipients at nearly 1/10th of the concentration in comparison to the smaller anionic molecules like phytic acid.

As the binding of anions to specific sites in DBF showed promising physical stabilization of the protein, we also investigated the effect of cationic excipients. DBF protein formulated with 0.5× and 10× concentration (by weight) of poly-arginine, 1,4-diaminobutane dihydrochloride (DABC or putrescine HCl) and protamine sulfate were analyzed using DSC and any change in Tm was monitored. As shown in Fig. 11, there was very little effect on the DBF protein's thermal stability. The T_{onset} values (Fig. 11C) were reduced with all three excipients suggesting that in presence of cations, the thermal unfolding is faster in comparison to the protein in its native environment or MOPS buffer. As shown in Fig. 11B, the Tm values in the presence of 0.5× poly-arginine concentration reduced stability by 0.8 °C and increased by 0.7 °C at 10× concentration. In contrast, the small cationic molecule, putrescine showed a small but significant stabilization effect by increasing the T_m by 0.2 °C and 1.2 °C at 0.5× and 10× concentration respectively. The data suggests that, despite having many anionic amino acids in the sequence, DBF lacks large cation-binding sites that could stabilize the protein further upon binding with cationic excipients. According to the observations above, cations must be interacting either by weakly increasing the overall stability of the DBF protein structure or by altering the free energy change associated with hydration of the newly exposed core after thermal unfolding.[31]

Phytic acid was modeled into two structures of IpaD and one structure of IpaB. One thousand independent Autodock Vina docking runs were performed for grids fully encompassing IpaD, proteolitically truncated IpaD, and IpaB. The top 1000 scoring poses clustered into 3 or 4 locations on each of the structures (Fig. 12). All of the proteins were also visually inspected for clusters of cationic residues, and an additional 3 sites were identified on the IpaB surface (Fig. 12). At the 13 sites identified across the three structures (see Supplemental Table S1), local docking was performed using the Extra Precision (XP) mode in Glide by Schrodinger. The highest scoring unique poses at each site were selected for full atom refinement of the ligand and any residue within 8 Å using Prime MMGBSA.

Though poses at each site had similar scores using AutoDock Vina, there was a wide range in Glide XP docking scores. Each structure had at least one site that had docking score below −8 kcal/mol, with several sites having moderately good docking scores between −7 and −8 kcal/mol, while some sites had a docking score as low as −2.7 kcal/mol. In general, the top scoring models at each site featured numerous hydrogen bonds between the phytic acid and the protein, as well as several internal hydrogen bonds within the phytic acid. What distinguished the high scoring from low scoring sites was salt bridge interactions. Sites with better scores could make three or four salt bridge interactions, while the sites with the worse scores were unable to make more than one (data not shown).

Excipient Screening

We used DSC as the assay of choice for excipient screening because of its robust nature. Several GRAS (generally regarded as safe) excipients from various amino acids, polyols, chelators, sugars, etc. were evaluated for their effect on melting temperature of DBF. In addition to anionic excipients, PS-80, poloxamer 188, and small cationic excipients (arginine HCl and Putrescine) showed stabilization effects by improving the T_m significantly (Fig. 13). In contrast, Trehalose, Sucrose, Glycerol, EDTA, NaCl, Glycine, Urea, etc. alone showed destabilization effects.

Conclusion

This work provides an improved understanding toward various degradation mechanisms and how such mechanisms can be analyzed. Unique impacts of forced degradation on the DBF protein analyzed by various biophysical tools should prove to be very critical in future formulation development and comparability assessment. Moreover, the stabilization effect of phosphate and other anionic excipients on DBF protein unveiled unique interaction mechanisms, which can be further exploited for formulating a stable DBF protein-based vaccine.

Supplementary Material

Refer to Web version on PubMed Central for supplementary material.

Acknowledgement

This project has been funded in whole or in part with Federal funds from the National Institute of Allergy and Infectious Diseases, National Institutes of Health, Department of Health and Human Services, under Contract No. HHSN272201800043C. Author also acknowledge help from Nicholas R. Larson and Ti Lu for their help with the graphing and data processing.

References

1. McCrickard LS, Crim SM, Kim S, Bowen A. Disparities in severe shigellosis among adults - Foodborne diseases active surveillance network, 2002–2014. BMC Public Health. 2018;18(1):221. [PubMed: 29415691]
2. Schroeder GN, Hilbi H. Molecular pathogenesis of Shigella spp.: controlling host cell signaling, invasion, and death by type III secretion. Clin Microbiol Rev. 2008;21(1):134–156. [PubMed: 18202440]
3. Chen X, Choudhari SP, Martinez-Becerra FJ, et al. Impact of detergent on biophysical properties and immune response of the IpaDB fusion protein, a candidate subunit vaccine against Shigella species.Infect Immun. 2015;83(1):292–299. [PubMed: 25368115]
4. Martinez-Becerra FJ, Kissmann JM, Diaz-McNair J, et al. Broadly protective Shigella vaccine based on type III secretion apparatus proteins. Infect Immun. 2012;80(3):1222–1231. [PubMed: 22202122]
5. Martinez-Becerra FJ, Scobey M, Harrison K, et al. Parenteral immunization with IpaB/IpaD protects mice against lethal pulmonary infection by Shigella. Vaccine. 2013;31(24):2667–2672. [PubMed: 23602665]
6. Heine SJ, Diaz-McNair J, Andar AU, et al. Intradermal delivery of Shigella IpaB and IpaD type III secretion proteins: kinetics of cell recruitment and antigen uptake, mucosal and systemic immunity, and protection across serotypes. J Immunol. 2014;192(4):1630–1640. [PubMed: 24453241]

7. Martinez-Becerra FJ, Chen X, Dickenson NE, et al. Characterization of a novel fusion protein from IpaB and IpaD of Shigella spp. and its potential as a pan-Shigella vaccine. Infect Immun. 2013;81(12):4470–4477. [PubMed: 24060976]
8. Hawe A, Wiggenhorn M, van de Weert M, Garbe JH, Mahler HC, Jiskoot W. Forced degradation of therapeutic proteins. J Pharm Sci. 2012;101(3):895–913. [PubMed: 22083792]
9. Wang T, Kumru OS, Yi L, et al. Effect of ionic strength and pH on the physical and chemical stability of a monoclonal antibody antigen-binding fragment. J Pharm Sci. 2013;102(8):2520–2537. [PubMed: 23824562]
10. Wei Y, Wahome N, Kumar P, Whitaker N, Picking WL, Middaugh CR. Effect of phosphate ion on the structure of lumazine synthase, an antigen presentation system from Bacillus anthracis. J Pharm Sci. 2018;107(3):814–823. [PubMed: 29045884]
11. Volkin DB, Tsai PK, Dabora JM, et al. Physical stabilization of acidic fibroblast growth factor by polyanions. Arch Biochem Biophys. 1993;300(1):30–41. [PubMed: 7678726]
12. Tadeo X, Lopez-Mendez B, Castano D, Trigueros T, Millet O. Protein stabilization and the Hofmeister effect: the role of hydrophobic solvation. Biophys J. 2009;97(9):2595–2603. [PubMed: 19883603]
13. Zangi R, Berne BJ. Aggregation and dispersion of small hydrophobic particles in aqueous electrolyte solutions. J Phys Chem B. 2006;110(45):22736–22741. [PubMed: 17092024]
14. Bostrom M, Tavares FW, Finet S, Skouri-Panet F, Tardieu A, Ninham BW. Why forces between proteins follow different Hofmeister series for pH above and below pI. Biophys Chem. 2005;117(3):217–224. [PubMed: 15963625]
15. Senske M, Constantinescu-Aruxandei D, Havenith M, Herrmann C, Weingartner H, Ebbinghaus S. The temperature dependence of the Hofmeister series: thermodynamic fingerprints of cosolute-protein interactions. Phys Chem Chem Phys. 2016;18(43):29698–29708. [PubMed: 27806138]
16. Barta ML, Guragain M, Adam P, et al. Identification of the bile salt binding site on IpaD from Shigella flexneri and the influence of ligand binding on IpaD structure. Proteins. 2012;80(3):935–945. [PubMed: 22423359]
17. Barta ML, Shearer JP, Arizmendi O, et al. Single-domain antibodies pinpoint potential targets within Shigella invasion plasmid antigen D of the needle tip complex for inhibition of type III secretion. J Biol Chem. 2017;292(40):16677–16687. [PubMed: 28842484]
18. Barta ML, Tachiyama S, Muthuramalingam M, et al. Using disruptive insertional mutagenesis to identify the in situ structure-function landscape of the Shigella translocator protein IpaB. Protein Sci. 2018;27(8):1392–1406. [PubMed: 29672980]
19. Sastry GM, Adzhigirey M, Day T, Annabhimoju R, Sherman W. Protein and ligand preparation: parameters, protocols, and influence on virtual screening enrichments. J Comput Aided Mol Des. 2013;27(3):221–234. [PubMed: 23579614]
20. Friesner RA, Banks JL, Murphy RB, et al. Glide: a new approach for rapid, accurate docking and scoring. 1. Method and assessment of docking accuracy. J Med Chem. 2004;47(7):1739–1749. [PubMed: 15027865]
21. Friesner RA, Murphy RB, Repasky MP, et al. Extra precision glide: docking and scoring incorporating a model of hydrophobic enclosure for protein-ligand complexes. J Med Chem. 2006;49(21):6177–6196. [PubMed: 17034125]
22. Halgren TA, Murphy RB, Friesner RA, et al. Glide: a new approach for rapid, accurate docking and scoring. 2. Enrichment factors in database screening. J Med Chem. 2004;47(7):1750–1759. [PubMed: 15027866]
23. Jacobson MP, Friesner RA, Xiang Z, Honig B. On the role of the crystal environment in determining protein side-chain conformations. J Mol Biol. 2002;320(3):597–608. [PubMed: 12096912]
24. Jacobson MP, Pincus DL, Rapp CS, et al. A hierarchical approach to all-atom protein loop prediction. Proteins. 2004;55(2):351–367. [PubMed: 15048827]
25. Choi KY, Min KH, Yoon HY, et al. PEGylation of hyaluronic acid nanoparticles improves tumor targetability in vivo. Biomaterials. 2011;32(7): 1880–1889. [PubMed: 21159377]

26. Micsonai A, Wien F, Kernya L, et al. Accurate secondary structure prediction and fold recognition for circular dichroism spectroscopy. Proc Natl Acad Sci U S A. 2015;112(24):E3095–E3103. [PubMed: 26038575]

27. Liu D, Ren D, Huang H, et al. Structure and stability changes of human IgG1 Fc as a consequence of methionine oxidation. Biochemistry. 2008;47(18):5088–5100. [PubMed: 18407665]

28. Kappel C, Luther K, Troe J. Shock wave study of the unimolecular dissociation of H2O2 in its falloff range and of its secondary reactions. Phys Chem Chem Phys. 2002;4(18):4392–4398.

29. Ami D, Lavatelli F, Rognoni P, et al. In situ characterization of protein aggregates in human tissues affected by light chain amyloidosis: a FTIR microspectroscopy study. Sci Rep. 2016;6:29096. [PubMed: 27373200]

30. Watkinson A, Soliakov A, Ganesan A, et al. Increasing the potency of an alhydrogel-formulated anthrax vaccine by minimizing antigen-adjuvant interactions. Clin Vaccine Immunol. 2013;20(11):1659–1668. [PubMed: 23986317]

31. Bye JW, Falconer RJ. Thermal stability of lysozyme as a function of ion concentration: a reappraisal of the relationship between the Hofmeister series and protein stability. Protein Sci. 2013;22(11):1563–1570. [PubMed: 24038575]

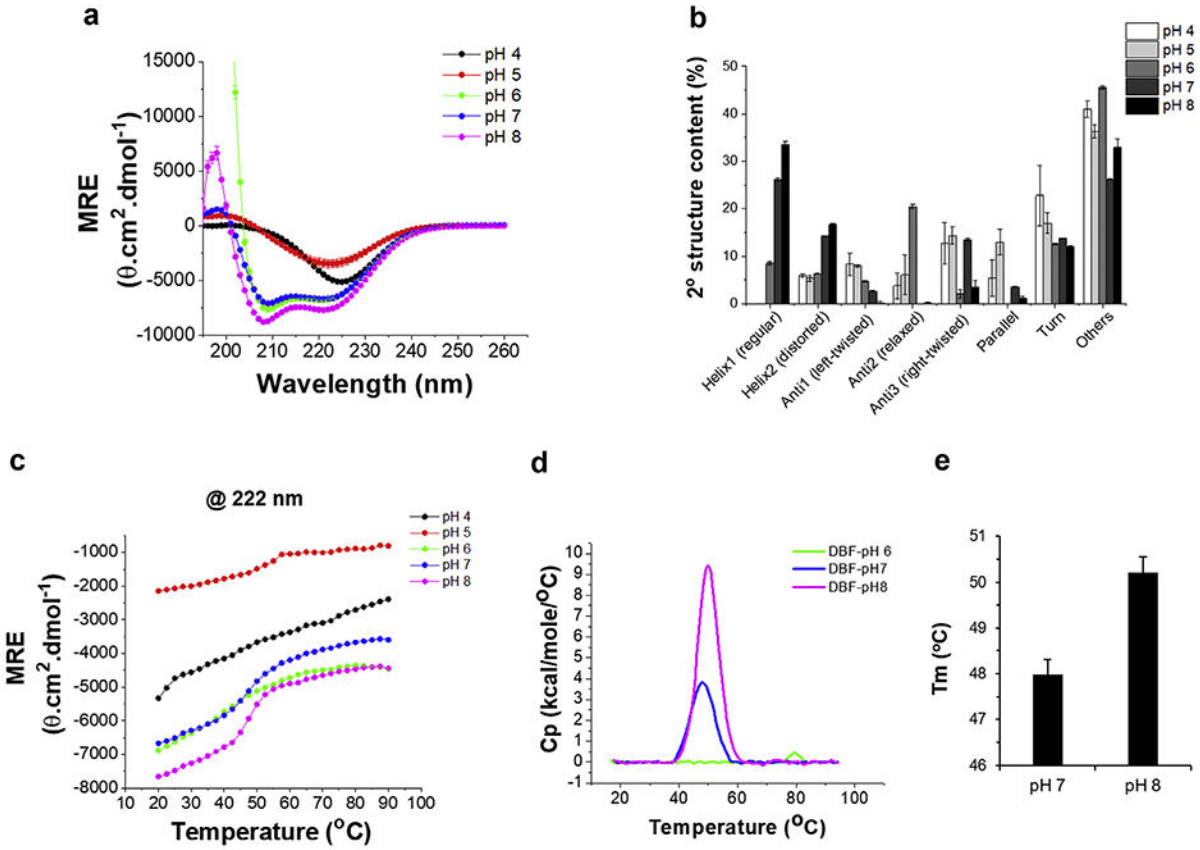

Fig. 1.

Effect of pH (4—8) on the conformational stability of DBF. (A) CD spectra of DBF in various pH conditions; (B) Secondary structure content of DBF in different pH conditions; (C) Mean Residue ellipticity at 222 nm plotted for DBF protein as a function of temperature; (D) Representative DSC thermograms of DBF protein at various pH; (E) Quantitated melting temperature of DBF at pH 7 and 8.

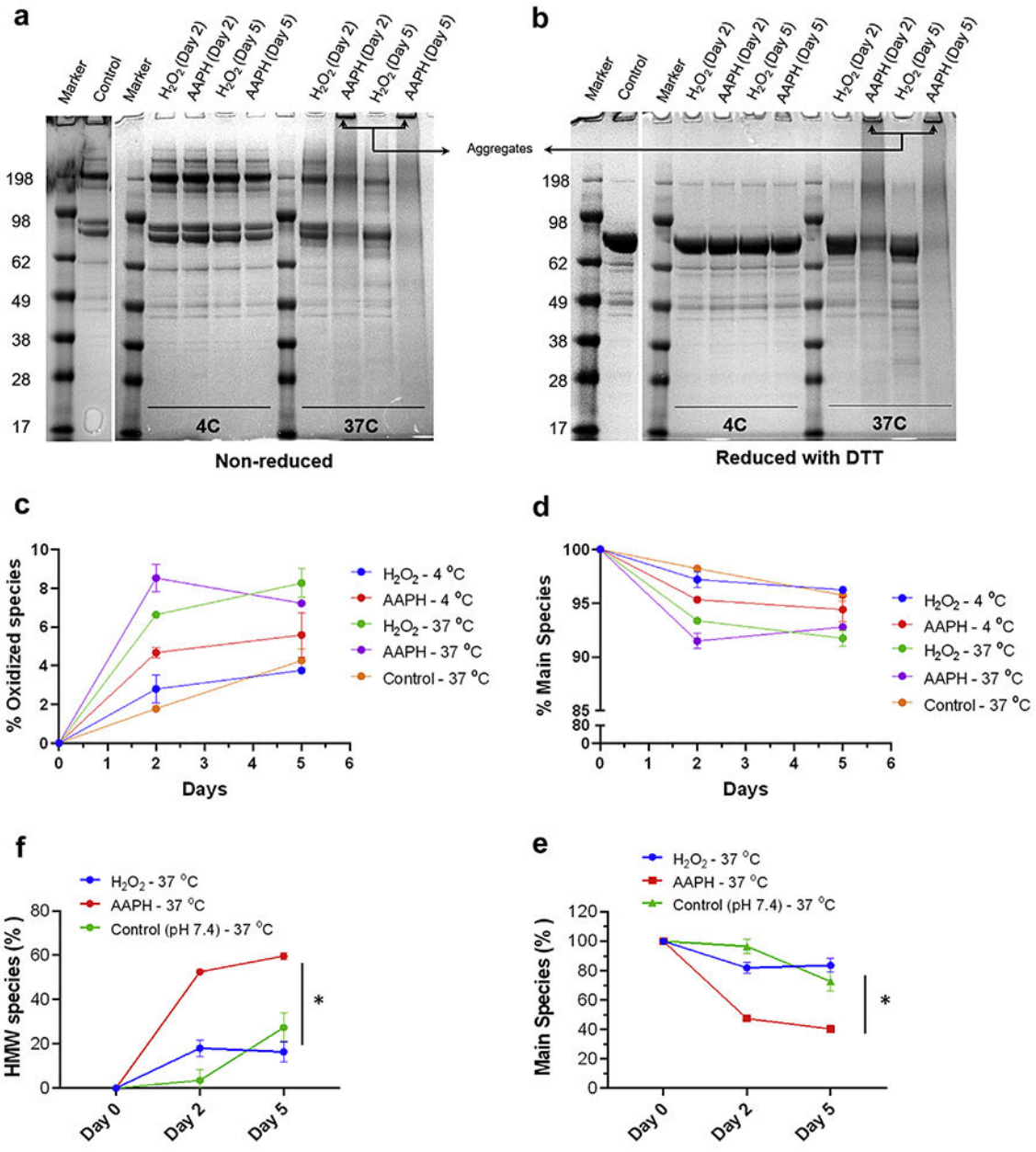

Fig. 2.

Forced Met and Trp oxidation of DBF in the presence of H_2O_2 and AAPH analyzed by (A) Non-reduced SDS-PAGE; (B) Reduced SDS-PAGE; (C) Percent oxidized species; (D) Percent main species evaluated by quantitating the area under the curve of the HIC chromatogram; (E) high molecular weight species, (F) main species, and (G) low molecular weight species respectively, quantitated from the area under the curve of SE-HPLC chromatogram.

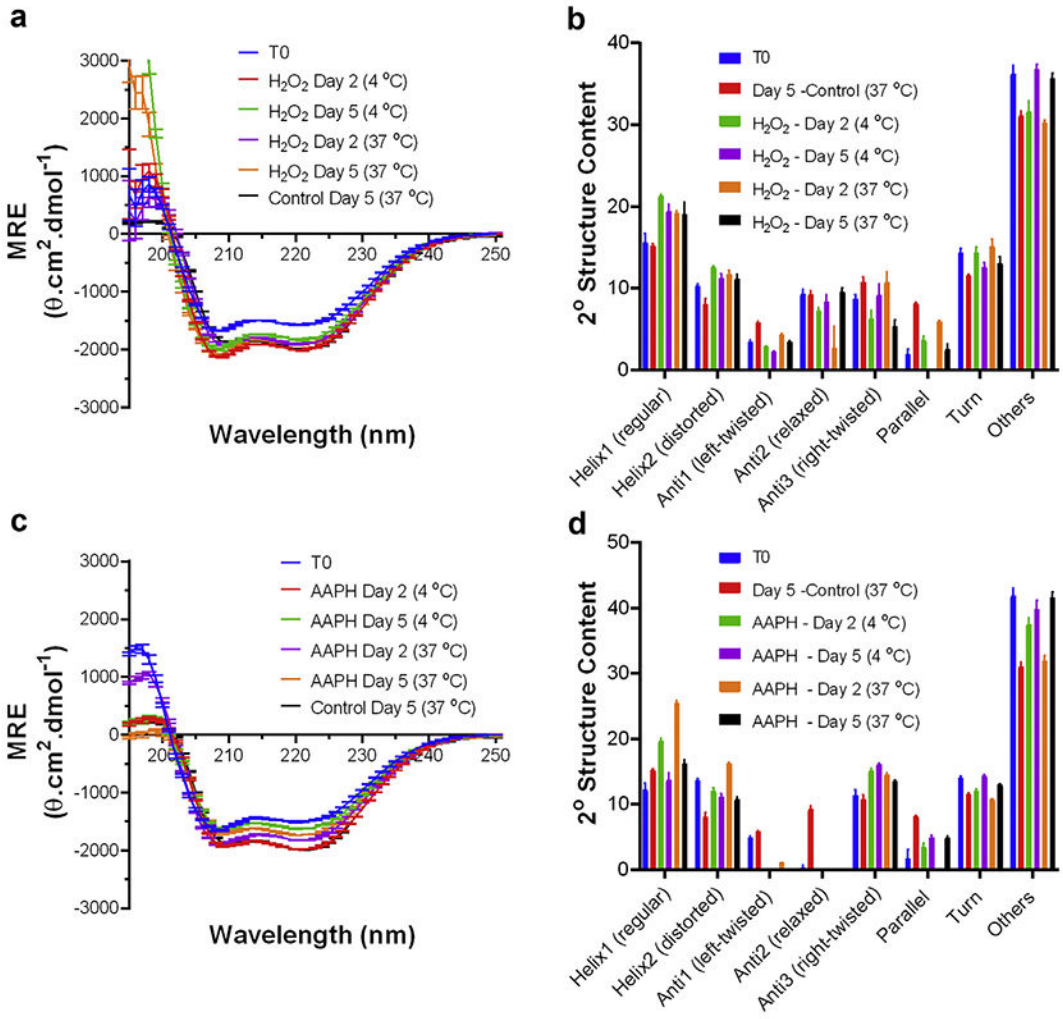

Fig. 3.

Effect of forced oxidation on the secondary structure of DBF at 4° and 37 °C for 2 and 5 days. A DBF control is designated as T_0. CD spectra of DBF oxidized by H_2O_2 (A) or AAPH (C); Secondary structure content of DBF after oxidation with H_2O_2 (B) or AAPH (D).

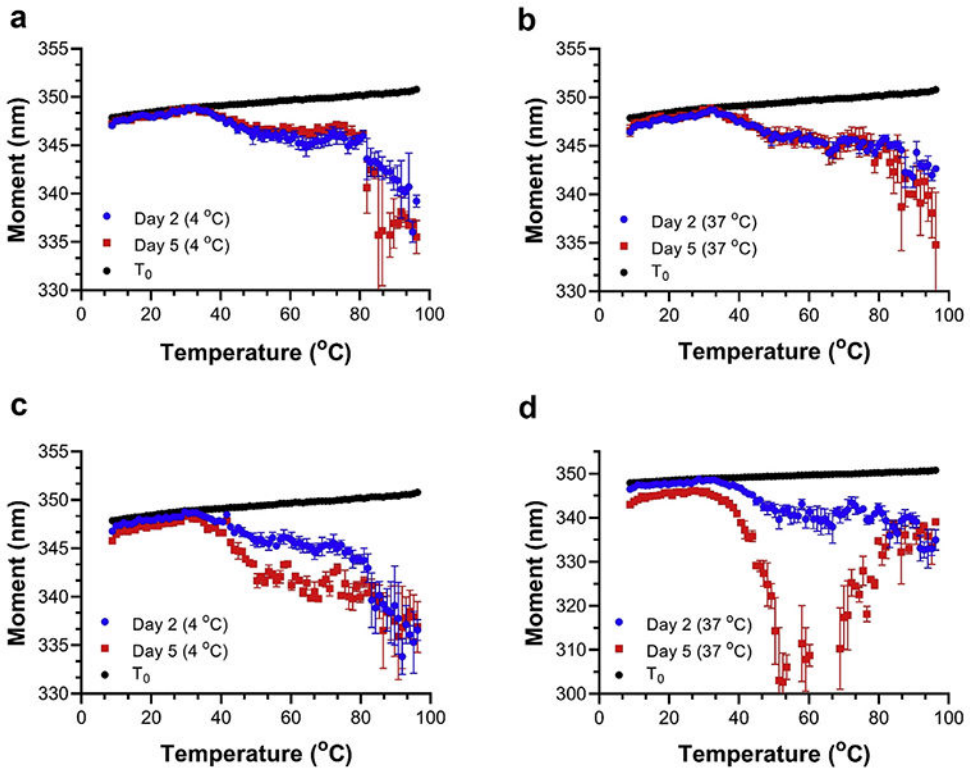

Fig. 4.

Effect of forced oxidation on the tertiary structure of DBF protein at various incubation conditions (days and temperature). The fluorescence moment is plotted as a function of temperature for DBF protein oxidized by (A) H_2O_2 at 4 °C, (B) H_2O_2 at 37 °C, (C) AAPH at 4 °C, (D) AAPH at 37 °C. The DBF control is indicated as T_0.

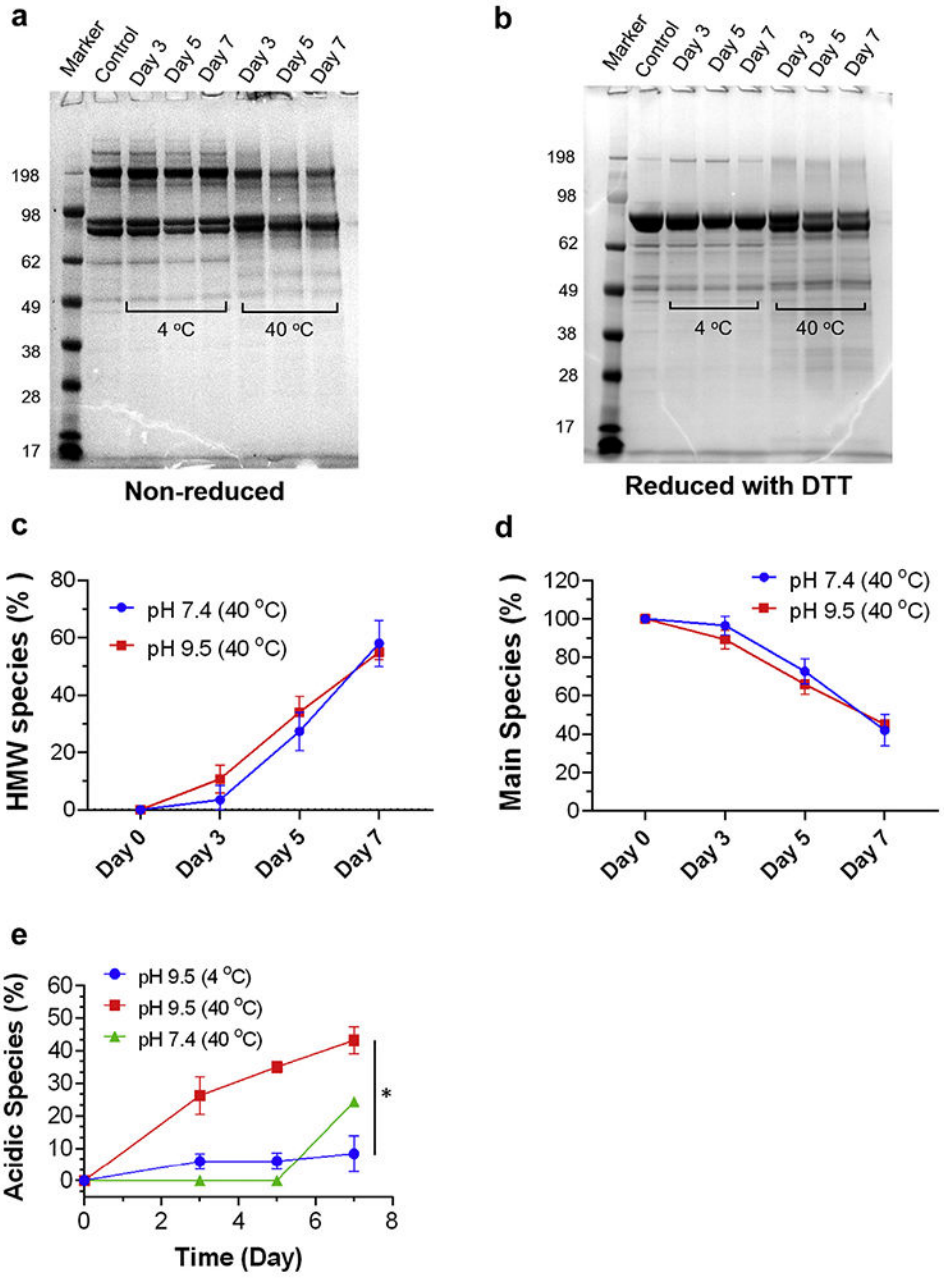

Fig. 5.

Forced Asn deamidation of DBF at pH 9.5 at 4 °C or 40 °C for 3, 5, and 7 days. (A) Non-reduced SDS-PAGE; (B) Reduced SDS-PAGE; (C) Percent of main species; (D) Percent of high molecular weight species; (E) Percent of low molecular weight species evaluated by quantitating the area under the curve of SE-HPLC chromatogram; (F) Percent of acidic species calculated by quantifying the area under the curve of the cIEF chromatogram from samples incubated under various conditions. DBF sample incubated with 10 mM MOPS, 0.05% LDAO, pH 7.4 at 40 °C was used as a control.

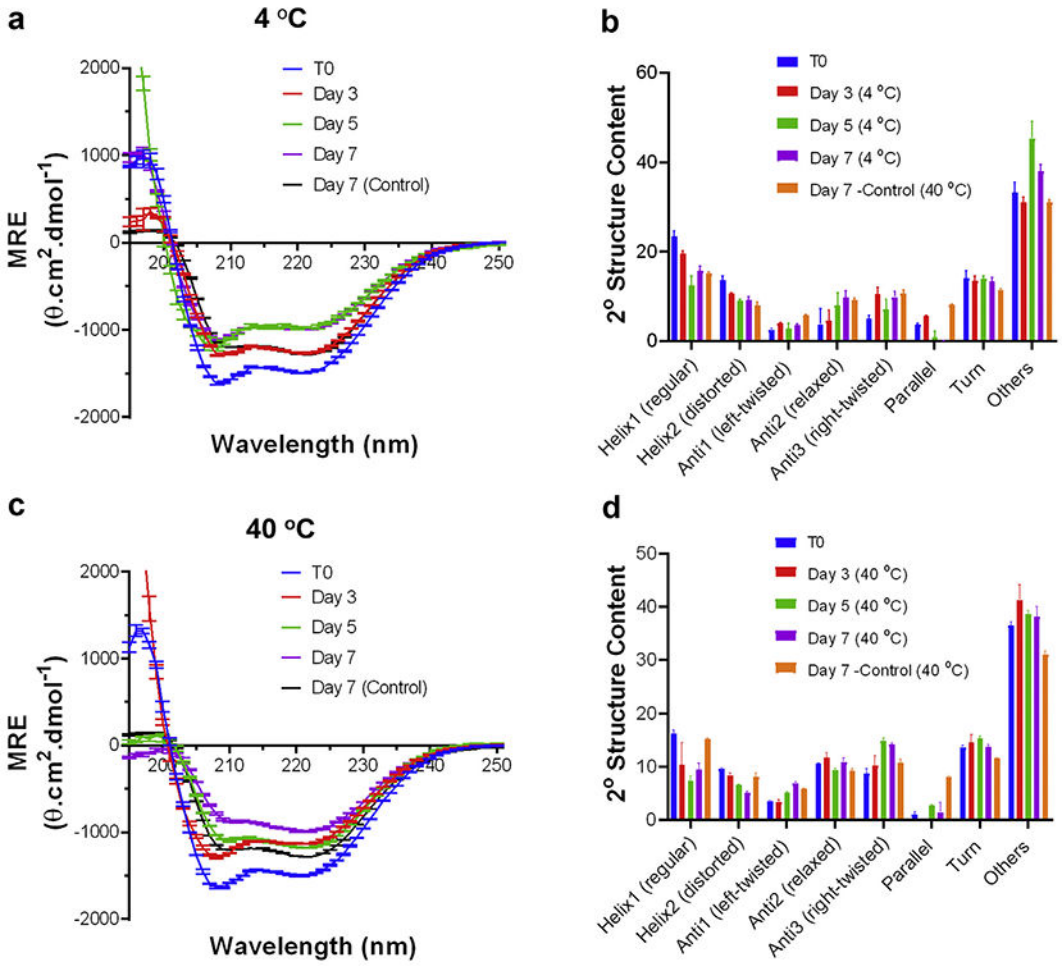

Fig. 6.

Effect of forced deamidation on the secondary structure of DBF at 4 °C and 40 °C for 3, 5, and 7 days. CD spectra of DBF deamidated at pH 9.5 at (A) 4 °C and (C) 40 °C; Secondary structure content of DBF protein after deamidation at pH 9.5 at (B) 4 °C and (D) 40 °C. A DBF control is used for comparison and marked as T_0.

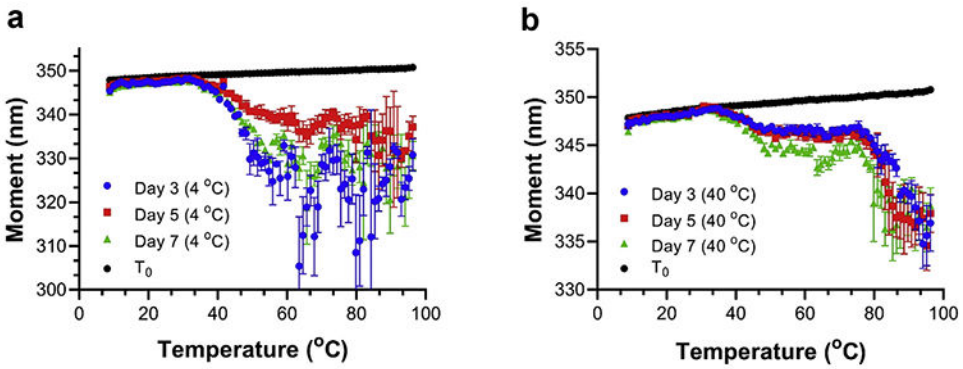

Fig. 7.

Effect of forced deamidation on the tertiary structure of DBF at various incubation conditions (Days and Temperature). The fluorescence moment is plotted as a function of temperature for DBF deamidated at (A) 4 °C, and (B) 40 °C. The DBF control is marked as T_0.

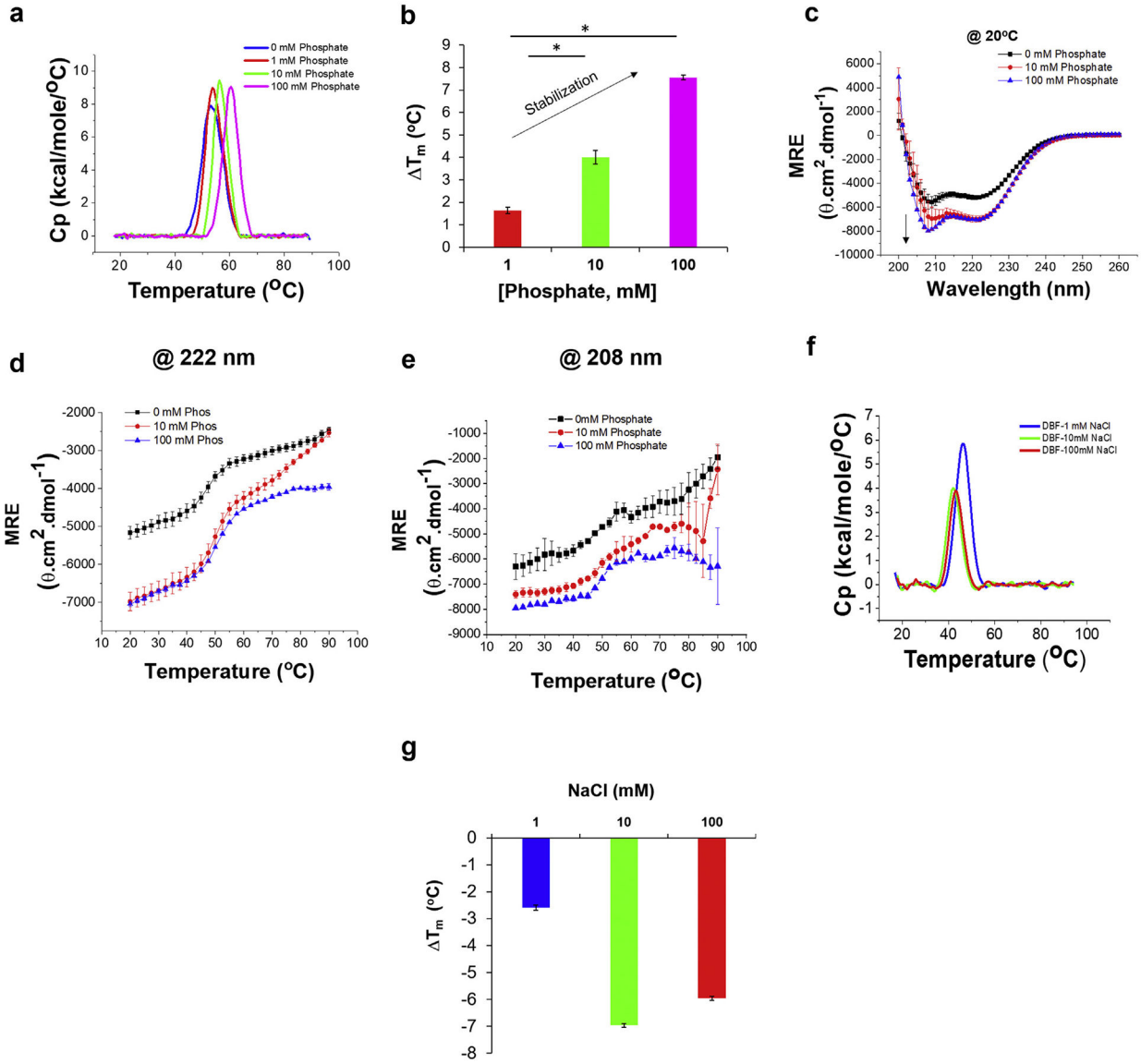

Fig. 8.

Effect of ionic strength of salts in the solution on the conformational stability of DBF. (A) A representative thermogram of DBF protein in presence of 1-, 10- and 100-mM phosphate. (B) The change in melting temperature (ΔTm) of DBF is shown as a function of the phosphate concentration in the solution. (C) CD spectra of DBF in the presence of 1-, 10- and 100-mM phosphate. (D) Molar residue ellipticity at 222 nm is plotted as a function of temperature. (E) Molar residue ellipticity at 208 nm is plotted as a function of temperature. (F) Representative thermograms of DBF are shown in the presence of 1, 10 and 100 mM NaCl. (G) Changes in melting temperature (ΔTm) of DBF as a function of NaCl concentration.

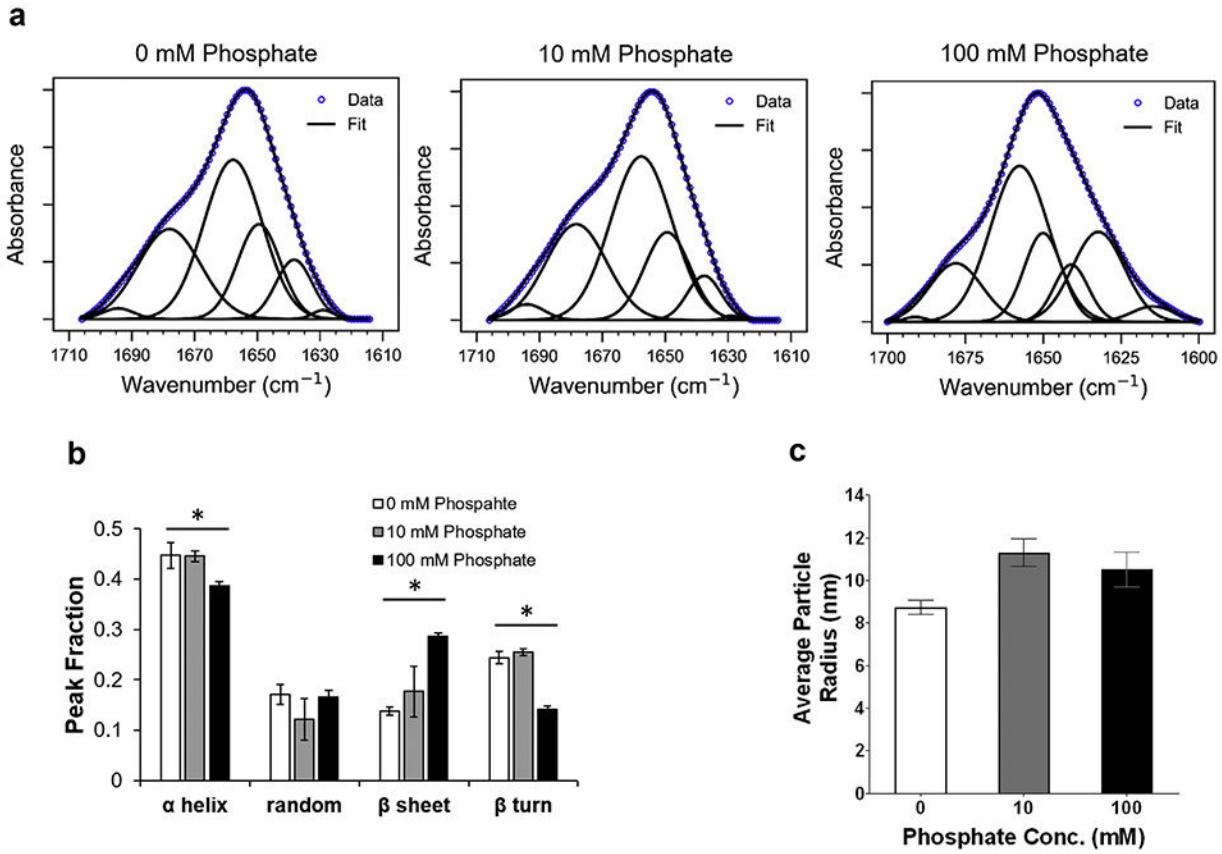

Fig. 9.

Effect of phosphate on the secondary and quaternary structure of the DBF protein. (A) Deconvoluted amide I region of FTIR spectra of the DBF in the presence of various phosphate concentrations; (B) Secondary structure content calculated for the DBF protein in presence of various phosphate concentrations; (C) Average particle size of DBF protein formulated at various phosphate concentrations.

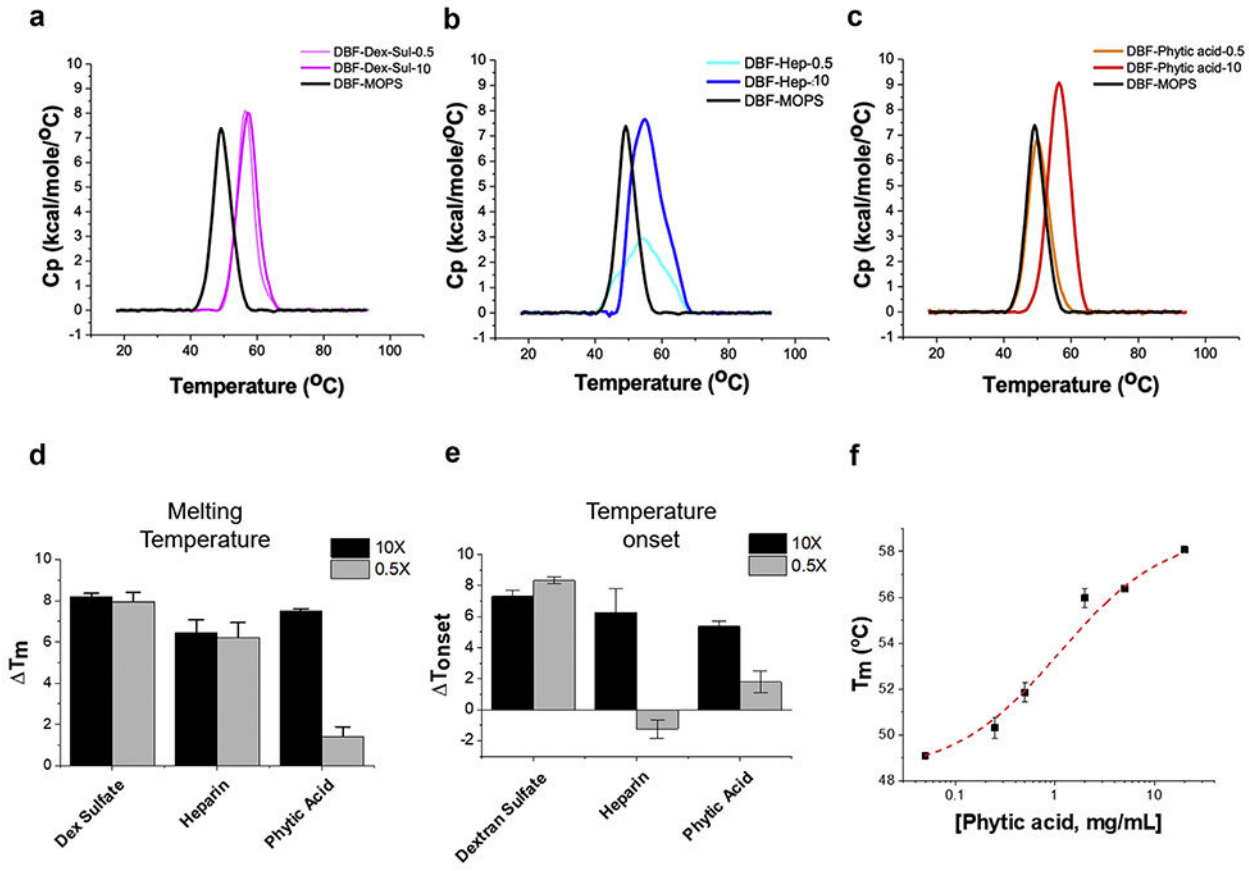

Fig. 10.

Effect of Anionic excipients on the stabilization of the DBF protein. Concentration normalized DSC thermogram of DBF in presence of 0.5× and 10× (by weight) of anionic excipients such as dextran sulfate (A), heparin sulfate (B), and phytic acid (C). (D) The change in Tm of DBF is shown with varying weight ratios of anionic excipients. (E) The change in T_{onset} of the DBF protein is shown with varying weight ratios of anionic excipients. (F) The melting temperature (Tm) of DBF is shown as a function of phytic acid concentration and monitored by differential scanning calorimetry.

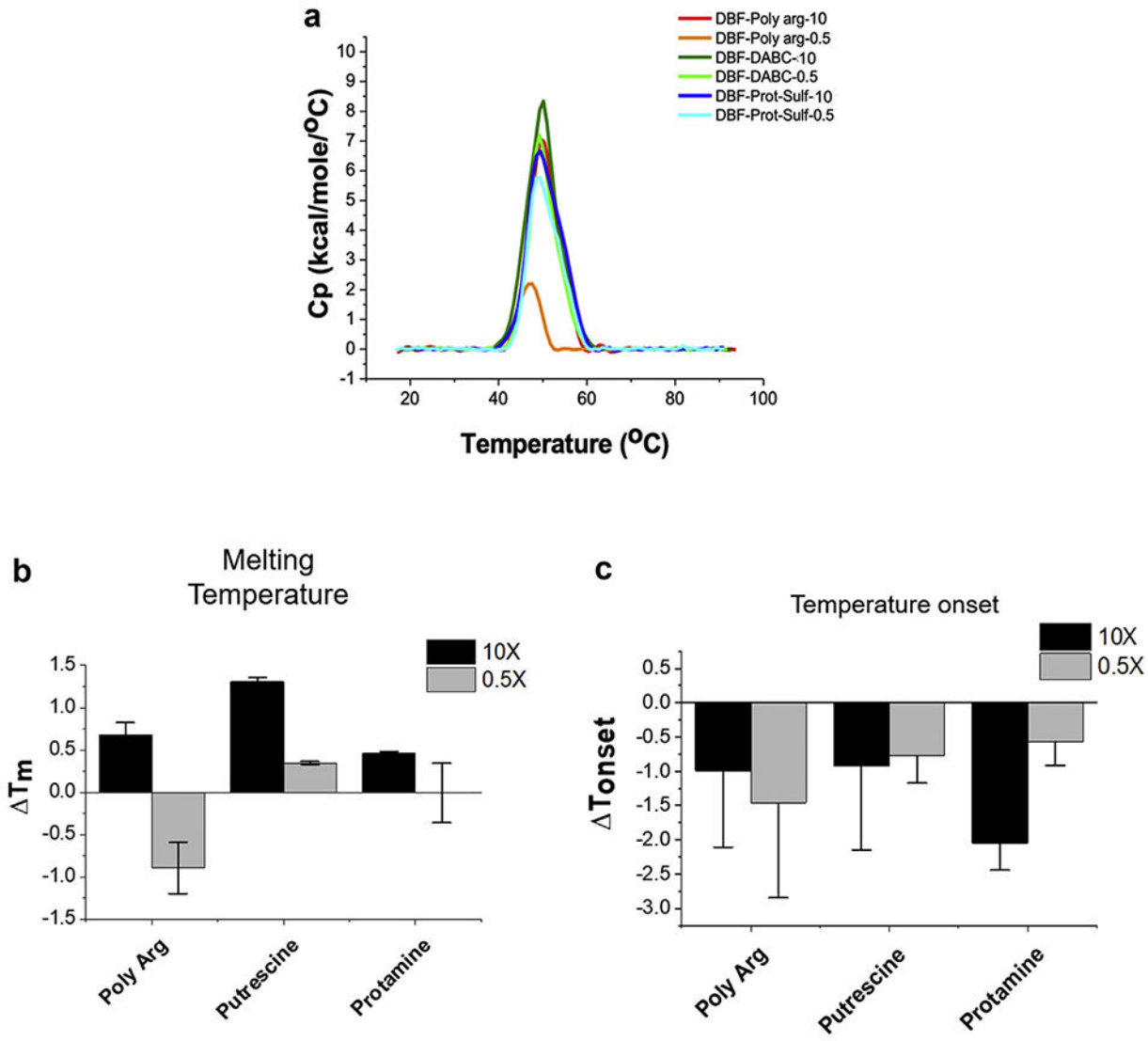

Fig. 11.

Effect of Cationic excipients on the conformational stabilization of the DBF Protein. (A) Concentration normalized DSC thermogram of DBF in the presence of 0.5× and 10× (by weight) of polyarginine, diaminobutane dihydrochloride (DABC or putrescine-HCl), and Protamine; (B) Change in Tm of DBF at varying weight ratios of cationic excipients; (C) Change in Tonset of the DBF protein with varying weight ratio of cationic excipients.

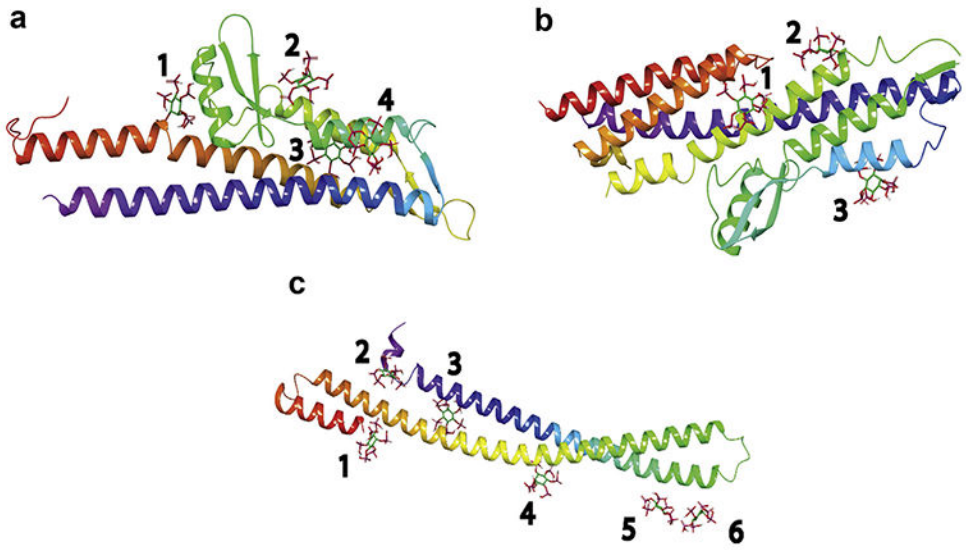

Fig. 12.

Potential phytic acid interaction sites on IpaD (A and B) and IpaB (C) identified by global docking and visual inspection. One thousand independent Autodock Vina runs were also performed against the proteolytically truncated IpaD structure (A) and its longer structure (B). The top one thousand poses clustered to 3 or 4 sites on the protein surface as shown. One thousand independent Autodock Vina runs were performed against IpaB (C). The top one thousand poses clustered to 3 sites on the protein surface (sites 1, 2, and 3). Visual inspection for clusters of positively charged amino acids identified three other sites (sites 4, 5, and 6).

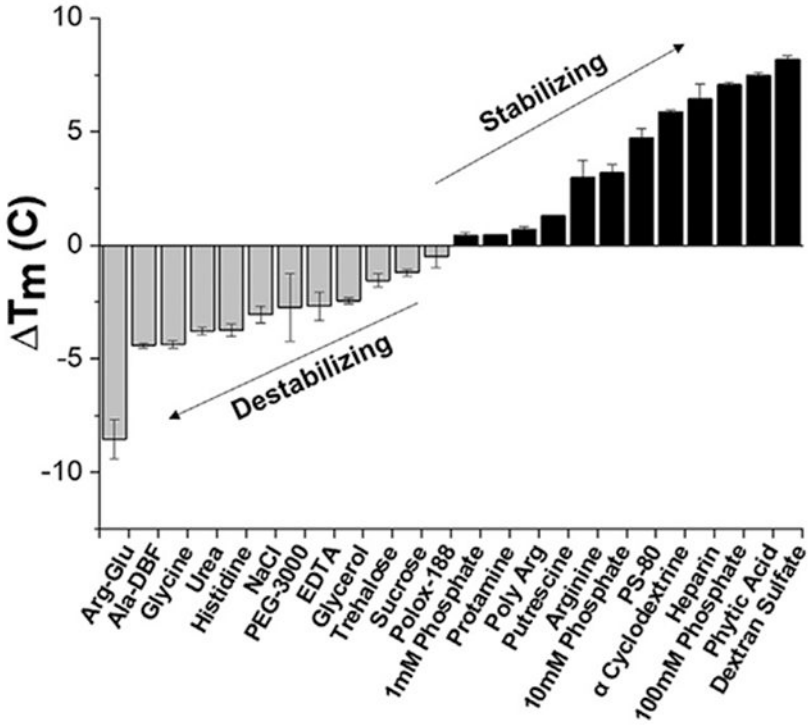

Fig. 13.

Excipient screening by monitoring thermal unfolding of DBF in the presence of various excipients. Average change in melting temperature (ΔTm) at which the folded and unfolded protein reach equilibrium are reported and ordered from excipient inducing lowest to highest stabilization.